Hindawi
Shock and Vibration
Volume 2022, Article ID 6536257, 11 pages
https://doi.org/10.1155/2022/6536257

Research Article

Analysis of Strengthening Mechanism of the Steep Slope Embankment through Centrifugal Model Test

Jie Liu,[1,2] **Bin Wang**,[1] **Yunlong Sun**,[1] **and Bin Wang**[2]

[1]*Xinjiang Agricultural University School of Transportation and Logistics Engineering, Urumqi 830006, China*
[2]*Xinjiang Transportation Planning Surveying and Design Institute, Urumqi 830006, China*

Correspondence should be addressed to Jie Liu; hfutliujie@163.com and Bin Wang; 1435654722@qq.com

Received 10 March 2022; Revised 3 June 2022; Accepted 6 June 2022; Published 14 July 2022

Academic Editor: Yonggang Zhang

Centrifuge model tests were conducted to investigate the geogrid-gravelly-soil-reinforced steep slope embankments. A control experiment was carried out on a set of unreinforced embankments. The following test results were obtained. Under a centrifugal force, the unreinforced gravelly soil steep embankments failed in sudden collapse and circular sliding. By contrast, the reinforced embankments exhibited a local deformation on the slope surface and a continuous progressive deformation on the slope due to the failure of geogrid-soil interface. The geogrid reinforcement strengthened the soil and enhanced the integrity of the embankment. Thus, the stability of the slope was improved, and the horizontal lateral displacement of the slope and the settlement at the slope crest were reduced. In the design of a geogrid, reinforcements should be sparsely arranged in the upper section of the embankment and densely arranged in the lower section. For equally spaced reinforcements, the geogrid should be strengthened in the middle and lower sections of the embankment.

1. Introduction

Due to their mechanical properties and reinforcing mechanism, geogrids are an effective way to reinforce and thus improve the properties of gravelly soil. A geogrid soil-reinforced steep slope embankment has excellent seismic resistance and reduces the slope angle, thereby decreasing both the amount of land needed for construction and ecological destruction. By mitigating difficulties in construction and hence shortening the construction period of projects, this type of embankment has become a very promising subgrade structure. However, the deformation and design theory of reinforced steep slope embankments is still immature, making it impossible to accurately analyze the deformation and failure mechanism of reinforced slopes.

In a centrifuge model test, increasing the gravitational field through high-speed rotation can make the stress-strain characteristics of a small-scale laboratory model test consistent with those of a prototype system, thereby intuitively and accurately capturing the mechanical properties of the prototype system. Therefore, the centrifuge model test offers a unique advantage for studying the deformation characteristics and failure mechanism of geogrid soil-reinforced steep slope embankments. Almeida et al. [1] studied the geogrid-reinforced piled embankment using numerical simulation and a centrifugal model. Through the centrifugal model tests, Balakrishnan and Viswanadham [2] evaluated the performance of geogrid-reinforced soil walls and studied the performance of the geosynthetic reinforced mixed slope with poor hydrophobic effect under rainfall (2019). Cui and Xiao [3] used a centrifugal model to study the embankment supported by geogrid-reinforced rammed earth and cement-soil columns on a soft soil foundation. Feng et al. [4] used a centrifugal model to study the performance of geogrid-reinforced piled embankment on a soft soil foundation. Kyparissis and Lopes [5] studied the bearing capacity of the reinforced soil under strip foundations using centrifugal model tests. Mamaghanian et al. [6] investigated the geocomposite reinforced soil walls under seepage using a centrifugal model test. Based on the centrifugal model and numerical model, Razeghi et al. [7] revealed the characteristics of an edge-backfilled geogrid-reinforced soil wall

with and without geocomposite layer. Shen et al. [8] evaluated the overall performance of a geotechnical synthetic fiber-reinforced pile embankment slope. Xu et al. [9], Xu et al. [10], and Zhang et al. [11] have carried out centrifuge model tests on reinforced slopes and reinforced retaining walls. The centrifuge model tests on the geogrid-gravelly-soil-reinforced steep slope embankment could show the strain pattern, deformation pattern, and failure mode of the geogrid and could reflect the key influencing factors. However, centrifugal model test on the reinforced gravel soil in a steep slope is not very common.

In the present study, centrifuge model tests were carried out on unreinforced and geogrid-gravelly-soil-reinforced steep slope embankments. Different reinforcement layer spacings were studied. The deformation pattern and failure mode of the geogrid-reinforced gravelly soil slopes were investigated. The rationality and structural safety of a design scheme for reinforced steep slope embankments, which is rarely used in engineering practice, were verified. The centrifuge model tests showed that geogrid reinforcement changed the failure mode of the slope. The geogrid barred the formation of a continuous sliding surface in the reinforced slope. The main failure modes were local deformation of the slope surface and continuous progressive deformation of the soil between the geogrid layers. These results are extremely significant in the rational selection of reinforcement layer spacing.

2. Experimental Procedure

2.1. Test Equipment. The CKY-200 multifunctional geotechnical centrifuge at the Yangtze River Scientific Research Institute was used in the tests. The main parameters were as follows: effective capacity, 200 g-t; maximum acceleration, 200 g; stepless speed regulation, with a speed regulation accuracy of 0.1 g; and maximum effective radius, 3.75 m. The deformation of the reinforced steep slope embankment can be approximated as a plane strain problem. The dimensions of the configured model box were 100 cm × 40 cm × 80 cm, as shown in Figure 1.

2.2. Experimental Model Design. The experimental prototype was a segment of a geogrid-gravelly-soil-reinforced steep slope embankment that will be constructed in the Shawan section of the S101 line. The prototype had a slope height of 10.67 m and a design slope ratio of 1 : 0.75. The subgrade was reinforced with a TGDG80HDPE geogrid. A two-dimensional (2D) model box with length × width × height dimensions of 1.0 m × 0.4 m × 0.8 m was selected. A model ratio of $n = 25$ was used, resulting in a scaled model height of 42.7 cm and a reinforcement length of 36 cm.

Four sets of tests were designed to analyze the influence of the reinforcement and different layer spacings on the stability of the geogrid-gravelly-soil-reinforced steep slope embankment models. The test schemes are shown in Table 1.

In the RS1 model, the safety factor of slope is 1.10, and the slope settlement and the horizontal displacement of the free surface of the slope were monitored. In the RS2 to RS4 models, the slope settlement and the horizontal displacement and geogrid strain of the free surface of the slope were monitored. The profile design of the models and the arrangement of the monitoring components are shown in Figure 2.

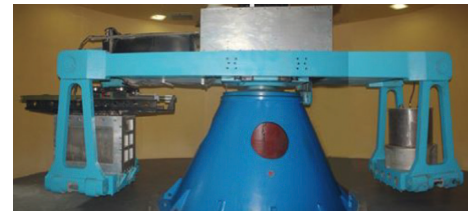

Figure 1: CKY-200 geotechnical centrifuge.

2.3. Material Modeling

2.3.1. Fill Material. In the geotechnical centrifuge test, the prototype specimen material was gravelly soil with the following properties: an optimum water content of 5.3%, a maximum particle size of 20 mm, a compactness of 0.93, a dry density of 1.93 g/cm^3, a cohesion c of 17.5 kPa, and an internal friction angle φ of 41.5°. The size effect of the gravelly soil particles was considered in the geo-centrifuge model tests because the ratio between the minimum dimension of the model box and the characteristic soil particle size affects the model deformation. Existing test results show that the influence of the model box boundary can be neglected when this ratio satisfies the following:

$$\left.\begin{aligned} \frac{B_{\min}}{d_{\max}} &> 13 \\ \frac{d_{50}}{B_{\min}} &> 60 \end{aligned}\right\}, \quad (1)$$

where $B_{\min}$ is the minimum dimension of the model box; $d_{\max}$ is the maximum particle size of the model specimen; and d_{50} is the average particle size of the model specimen.

The maximum allowable particle size in the model box was 20 mm, and the average particle size was limited to 6.67 mm. The supersized particles were graded and scaled by replacement with an equal proportion of coarse particles that were smaller than the maximum particle size allowed by the minimum dimension of the model box.

2.3.2. Geogrid. In the reinforced soil structure, the geogrid stress is much lower than the geogrid fracture strength, and the geogrid strain is generally less than 2%. The modulus of the geogrid is generally close to that in the linear stage during normal use, and tensile failure of the geogrid is rarely seen in collapsed reinforced soil projects. Therefore, the main consideration in selecting substitute materials for a geogrid is that the principle of strain similarity should be met at a strain of 2%.

In the centrifuge model tests, reinforcing materials are generally simulated by polypropylene biaxial geogrid [9],

Table 1: Different centrifuge model test schemes.

No.	Test scheme	Spacing between geogrid layers (cm)
RS1	Centrifuge model test on unreinforced gravelly soil steep slope embankment	
RS2	Centrifuge model test on geogrid-gravelly-soil-reinforced steep slope embankment based on prototype	5.0
RS3	Same as RS2, except with increased geogrid spacing (from 5.0 cm to 7.5 cm)	7.5
RS4	Same as RS2, except with increased geogrid spacing (from 5.0 cm to 10.0 cm)	10.0

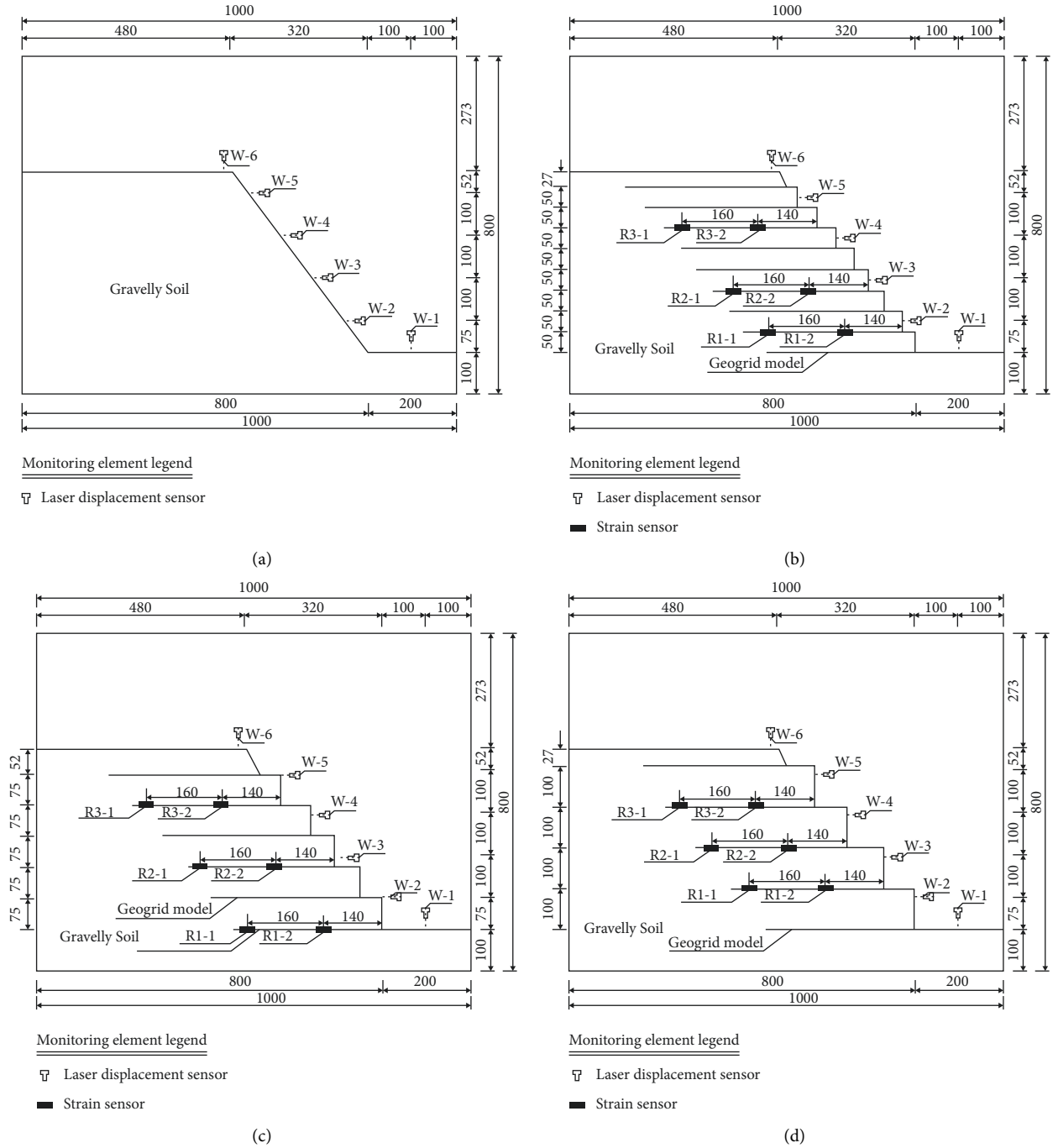

Figure 2: Arrangement of monitoring sensors in centrifuge models (unit: mm). (a) RS1. (b) RS2. (c) RS3. (d) RS4.

nonwoven polypropylene geotextile [12], and polyamide mesh [10]. In the present study, a polyamide mesh with an 1.2-mm spacing was selected as the geogrid model material. A tensile testing machine for geosynthetics was used to carry out a wide strip tensile test. The selected material had a tensile strength of 9 kN m and tensile forces of 0.87 kN/m and 2.51 kN/m at elongations of 2% and 5%, respectively. The reinforcement-soil interface coefficient of the geogrid model was 0.83, which was similar to that (0.8-0.9) obtained for the prototype material by a drawing test.

2.4. Model Development. The density control method was used to ensure the quality and test accuracy of the fill, and layer-by-layer compaction was performed with a layer thickness of 3 to 5 cm. After completion of the foundation, the slope surface formwork was installed layer by layer. Layer-by-layer compaction was performed during filling. The geogrid was placed at predetermined locations with proper tensioning. The formwork was removed after the model was filled to the top.

Resistive strain gauges were directly attached to the geogrid model to monitor the strain distribution characteristics of the geogrid. Noncontact laser displacement meters were mounted on special holders to monitor the slope displacement (Figure 3).

2.5. Design of Test Loading Procedures. The model prototype was a geogrid-gravelly-soil-reinforced steep slope embankment that was designed according to the grade 3 road standard. The design traffic load was 15.6 kPa. Based on similarity theory, the traffic load was simulated by laying an 8.0-mm-thick steel plate within the range of a 29-cm-wide roadway at the top of the model. Three loading stages were considered: a construction stage (during which the acceleration was gradually increased to 25 g over 20 min after the start of the test), an operational stage (stable operation for 6 min at an acceleration of 25 g), and an ultimate failure stage (during which the acceleration was increased stepwise from 25 g to 60 g). The acceleration loading curve is shown in Figure 4.

Simulation of construction phase: at the beginning of the test, the acceleration was gradually increased to 25 g within 20 minutes to simulate the construction period. Starting from an acceleration of 10 g, after ensuring the horizontal operation of the centrifuge model box, it ran for 6 minutes with an increment of 10 g for the first-stage acceleration. The increment of the second-stage acceleration was kept at 5 g, until reaching the operation stage. Simulation of operation stage: stable operation was maintained with 25 g acceleration for 6 minutes to simulate the operation period. At this time, the self-weight and driving load of the model are consistent with those of the prototype. Simulation of destruction stage: the destruction stage was simulated by continuously increasing the centrifugal acceleration. In the destruction stage, the increment of the first-stage acceleration was 15 g and was kept for 6 minutes. The increment of the second-stage acceleration was 20 g, and the acceleration was increased to the maximum of 60 g and was kept until the failure of the embankment slope. The failure mode at a limit state when the model was subjected to very high accelerations was simulated.

3. Test Results

3.1. Test Results for Unreinforced Embankment Model. When the acceleration was 25 g, the vertical displacement of the slope foot foundation was 53.95 mm. Due to an interference of the collapsed soil mass on the slope, effective data about the slope foot could not be monitored. The displacement of slope top increased with the acceleration. When the acceleration was 25 g, the top displacement was 150.58 mm; when the acceleration was 32 g, the soil on the upper part of the slope suddenly collapsed. Due to an influence of the slope slump, effective data at $W1$ could not be monitored. The displacement of $W6$ varied from 100 mm to 124 mm. The displacements of the slope top and the foundation at slope foot increased with the acceleration g.

The horizontal displacement at the slope monitoring point increased continuously with the acceleration. With an acceleration of 25 g, the displacements of the model slope to free surface were 35.74 mm ($W2$), 17.89 mm ($W4$), and 74.45 mm ($W5$), respectively. With the continuous increase of acceleration, the settlement occurred at the slope top and the overall deformation of the slope and foundation also continued to increase, which was an unstable slope. When the acceleration was 32 g, the horizontal displacement at measuring point $W5$ increased from 110 mm to 131 mm, and the slope rapidly entered the failure stage from an elastic-plastic deformation stage. When the acceleration increased to 38 g, the slope collapsed in a large range. When the acceleration continued to increase to 60 g, no any obvious large-scale collapse occurred on the slope.

In the early stage of the centrifugal test, a local shallow collapse occurred after the soil particles on the slope moved and became unstable. The collapse occurred when the acceleration increased from 20 g to 30 g. The main manifestations are that the settlement of slope top continuously increased, an obvious uplift of the foundation at slope foot occurred, and the lateral displacement of the slope occurred toward the free surface and then the slope collapsed. A typical arc-shaped sliding surface was formed in the upper 3/4 of the slope (Figure 5).

3.2. Centrifuge Model Test Results of Reinforced Embankments

3.2.1. Slope Shape and Displacement Variation. RS2 to RS4 were geogrid-gravelly-soil-reinforced steep slope embankment models with different layer spacings. The upright step of the slope surface that existed before the test became circular after the test. However, from the start to the end of the test, for all three sets of reinforced embankment models, no overall slope failure occurred, and no overall sliding surface penetration through the reinforcement layers was observed (Figure 6).

The displacement data obtained at the toe, crest, and surface of the slope in the RS2 model are shown in Figure 7.

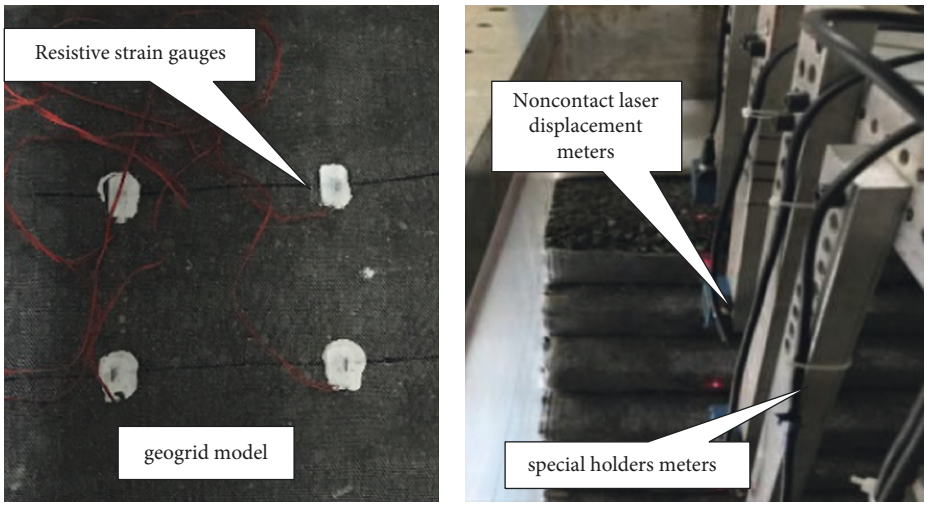

Figure 3: Installation of monitoring components. (a) Strain gauge. (b) Laser displacement sensor.

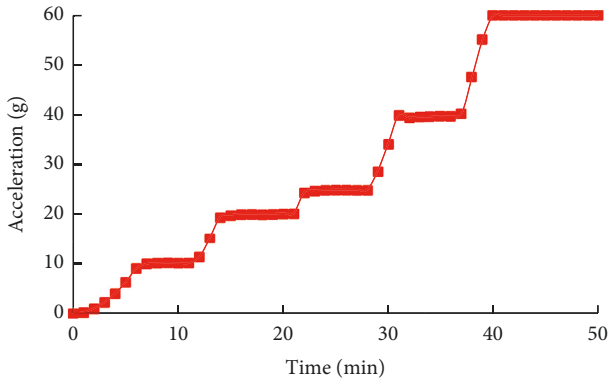

Figure 4: Acceleration versus time.

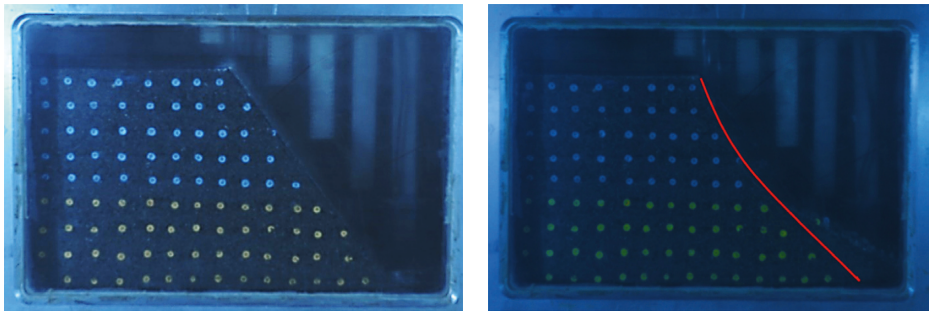

Figure 5: Photographs of centrifuge model test on embankment RS1 (a) before the test and (b) after the test.

The displacement of the monitoring point W-1 first increased and then decreased with increasing acceleration. In the early stage, consolidation settlement of the slope occurred under centrifugal acceleration, and in the late stage, the toe of the slope lifted up, and the displacement decreased. After the centrifuge model was tested at an acceleration of 25 g for 5 min, the shoulder of the subgrade slope settled by 1.98 mm. This centrifugal model test ratio is $n = 25$, and the similarity relation was used to determine the settlement at the crest of the prototype slope as 49.5 mm.

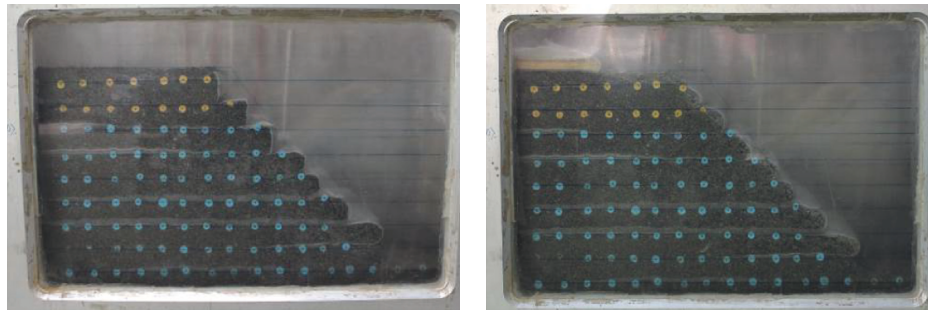

(a) (b)

Figure 6: Photographs of centrifuge model test on embankment RS2 (a) before the test and (b) after the test.

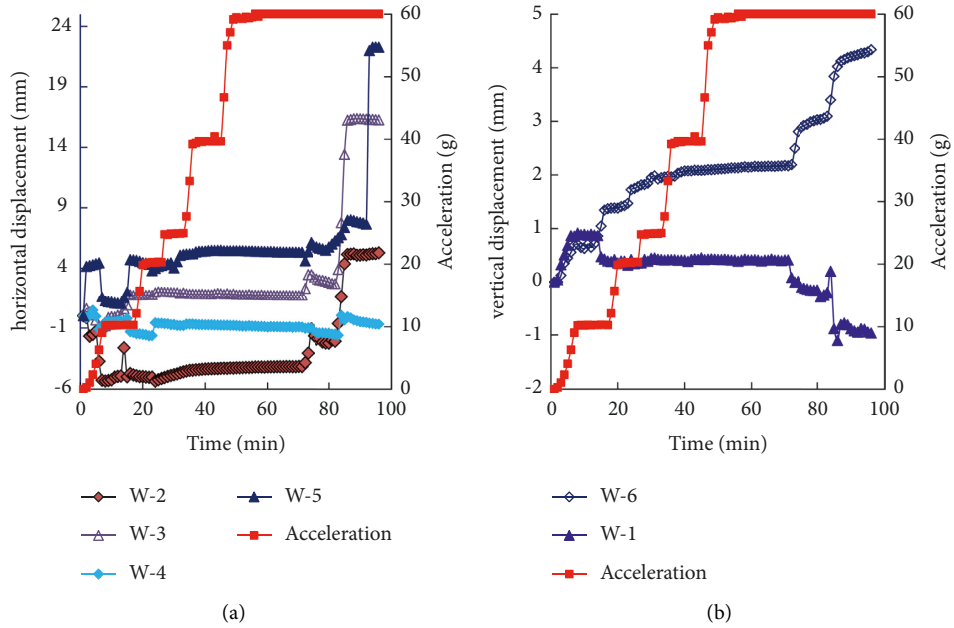

(a) (b)

Figure 7: Displacement variation curves of RS2 model. (a) Slope surface displacement. (b) Settlements of the slope crest and toe.

After the centrifuge model was tested at an acceleration of 25 g for 5 min, the displacements of the slope surface were 4.58 mm (W-2), 0.80 mm (W-3), −1.95 mm (W-4), and −5.14 mm (W-5). Under centrifugal acceleration, the soil between two geogrid layers that was in an upright position during the model construction slid within a small range after the start of testing (Figure 6). After testing at 60 g for 30 min, a large, abrupt change in the displacement occurred at each of the positions W-1 to W-6 on the slope of the centrifuge model, with the maximum displacement (–13.41 mm) occurring in the middle-upper section (W-4) of the slope. The settlement at the crest of the slope increased from 1.95 mm to 3.84 mm. At the same time, a slight settlement also occurred in the foundation at the toe of the slope. However, failure by slope instability did not occur, mainly because the separation of the geogrid prevented the coalescence of the sliding surface formed in the soil.

The displacement data obtained at the toe, crest, and surface of the slope in the RS4 model are shown in Figure 8. After the model was tested at an acceleration of 13 g for 13 min, the shape of the slope surface changed suddenly. After the centrifuge model was tested for 31 min, the acceleration was increased to 25 g. After testing the model for 5 min, the foundation at the toe of the slope (W-1) settled by −0.65 mm, the ground lifted up, and the shoulder of the subgrade slope (W-6) settled by 2.78 mm. After the model was tested for 53 min, the acceleration was increased to 60 g. After testing the model for 8 min, the foundation at the slope toe (W-1) settled by −0.57 mm, and the shoulder of the subgrade slope (W-6) settled by 4.96 mm. The vertical displacement at W-1 first increased and then decreased with the increase in the acceleration. Under centrifugal acceleration, the slope exhibited consolidation settlement, followed by uplift. The displacements of the slope surface were −16.86 mm (W-2), −14.55 mm (W-3), −12.62 mm (W-4), and −12.37 mm (W-5). Compared with the displacement after 31 min, the lateral displacements above the middle section of the slope (W-4 and W-5) were relatively smaller because of local sliding of the soil between the geogrid layers in the middle and upper sections of the slope. The uplift of

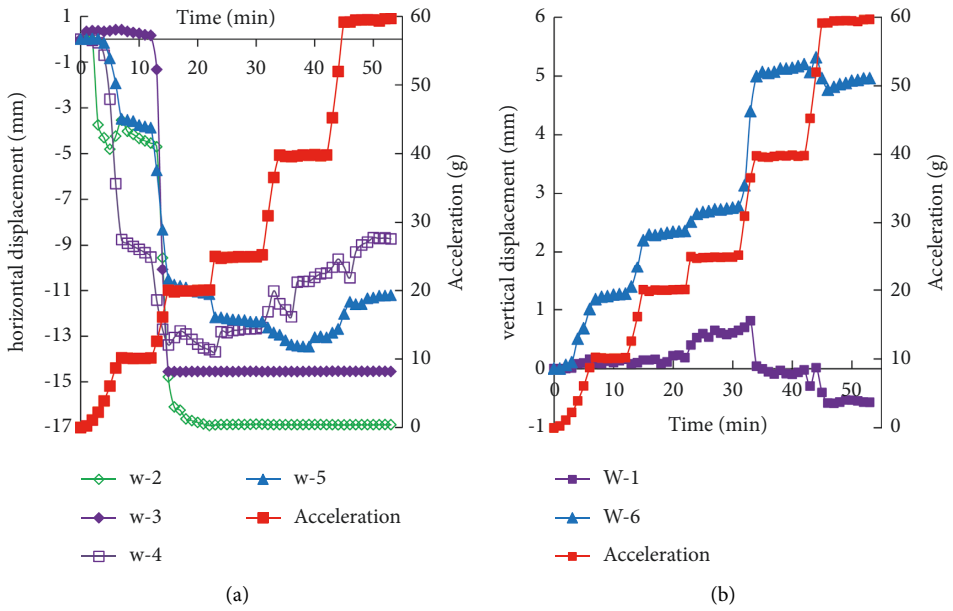

Figure 8: Displacement variation curves of RS4 model. (a) Slope surface displacement. (b) Settlements of slope crest and toe.

the foundation at the toe of the slope and the continuous deformation of the crest and the free surface of the slope indicated the progressive failure of the slope at 25 g.

The main changes in the shape of the slope surface before and after the centrifuge tests on the RS2 and RS4 models are presented here. The crest of the slope settled, and the soil between the two layers of the geogrid at the slope surface collapsed slightly. However, the overall slope did not collapse suddenly, and no cracking of the surrounding soil or tensile failure of the geogrid in the reinforcement model was observed. The displacement mainly consisted of the deformation of the wrapped-around soil and the nearby soil. Under the same acceleration, the crest settlement and surface displacement of RS2 were smaller than those of the RS3 and RS4 models with larger layer spacings. Thus, for small layer spacings, the geogrid reinforcement constrained the horizontal lateral displacement of the slope soil, which improved the slope stability.

3.2.2. Geogrid Strain Analysis. Figure 9 shows that after the RS2 centrifuge model was tested at 25 g for 5 min, the strains measured by the strain sensors were 0.192×10^{-3} ($R1$-1), 0.514×10^{-3} ($R1$-2), 0.797×10^{-3} ($R2$-2), 0.764×10^{-3} ($R3$-1), and 0.661×10^{-3} ($R3$-2). Note that data were not measured by sensor $R2$-1 in the middle section of the slope. At the monitoring points far away from the slope, the geogrid strain in the upper section was larger than that in the lower section. At the monitoring points close to the slope, the largest geogrid strain occurred in the middle section, followed by the upper section, whereas the smallest strain occurred in the bottom section. After testing the model at 60 g for 30 min, there was an abrupt change in the strain of the upper geogrids that was immediately followed by changes in the middle geogrids. The lower geogrids were the last to show an abrupt change, corresponding to the least amount of change.

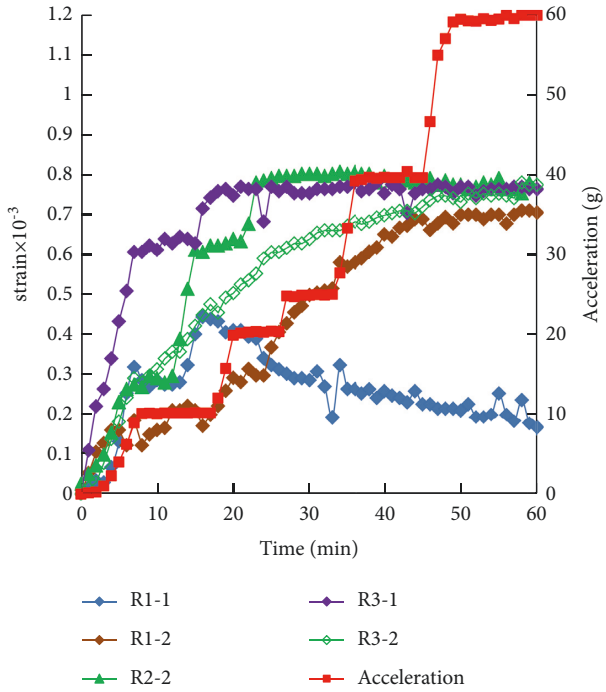

Figure 9: Geogrid strain in RS2 model.

In particular, large abrupt changes occurred at $R2$-2 and $R3$-1. The appearance of geogrid strains indicated that, under large gravity acceleration, the models proceeded from the plastic deformation stage to a failure stage. Thus, the soil in the slope had already undergone plastic failure, and the sliding force was resisted by the geogrids.

The geogrid layer of the RS3 centrifuge model was 7.5 cm long. The noncontact laser displacement sensor holder failed, resulting in abnormal monitoring data from the

displacement sensor. Only the microstrain of the geogrid was measured in the RS3 reinforced steep slope centrifuge model. The variation in the geogrid strain was very regular and consistent with that of centrifugal acceleration.

After testing the RS3 centrifuge model at 25 g for 5 min, the monitored strains were 1.601×10^{-3} ($R1$-1), 1.063×10^{-3} ($R1$-2), 0.665×10^{-3} ($R2$-1), 0.272×10^{-3} ($R2$-2), and 0.371×10^{-3} ($R3$-1), as shown in Figure 10. Data were not monitored by sensor $R3$-2.

At 60 g, the strains were 4.162×10^{-3} ($R1$-1), 3.147×10^{-3} ($R1$-2), 1.244×10^{-3} ($R2$-1), 0.961×10^{-3} ($R2$-2), and 1.013×10^{-3} ($R3$-1). In the RS3 embankment model, the microstrain of the geogrid increased with the acceleration. At the monitoring points far away from the slope, the geogrid strain in the bottom section was significantly larger than those in the middle and upper sections, and the geogrid strain in the middle section was slightly larger than that in the upper section. At the monitoring points close to the slope point, the geogrid strain in the bottom section was larger than that in the middle section. A comparison with the RS2 model strains showed that increasing the geogrid spacing significantly altered the geogrid stress distribution. A relatively large geogrid spacing considerably increased the microstrain of the geogrid, indicating that the geogrids in the lower section were subjected to higher tension.

The RS4 centrifuge model had a very large 10-cm spacing between the geogrid layers. The test lasted for 53 min, and the shape of the slope after the test is shown in Figure 11.

At the beginning of the RS4 model test, the strain of the geogrid near the middle section and close to the slope increased continuously with the acceleration and remained stable after the acceleration increased to 20 g. This result showed that the geogrid in the middle section of the slope began to withstand a large load at a relatively early stage. After being tested for 31 min, the centrifuge model was further tested at 25 g for 5 min. The geogrid strains in the slope were 1.517×10^{-3} ($R1$-1), 1.304×10^{-3} ($R1$-2), 0.153×10^{-3} ($R2$-1), 0.594×10^{-3} ($R2$-2), 0.262×10^{-3} ($R3$-1), and 0.190×10^{-3} ($R3$-2). In the RS4 embankment model, at the monitoring points far away from the slope, the geogrid strain in the bottom section was significantly larger than those in the middle and upper sections, which were very close to each other. After testing the model for 53 min, the acceleration was increased to 60 g, and the strains were 2.533×10^{-3} ($R1$-1), 1.605×10^{-3} ($R1$-2), 0.640×10^{-3} ($R2$-1), 0.551×10^{-3} ($R2$-2), 0.687×10^{-3} ($R3$-1), and 0.720×10^{-3} ($R3$-2). The microstrain of the geogrid increased with the acceleration, as for the RS3 model, indicating that the excessively large geogrid layer spacing led to excessive deformation of the structure and even instability from overall failure, as shown in Figure 12.

A comparative analysis was performed on the results of the three test sets, RS2, RS3, and RS4. At the monitoring points close to the slope, when the acceleration was less than 20 g, the largest geogrid strain was found in the middle section, the smallest strain was found in the upper section, and an intermediate strain was found in the middle section. However, there was no large difference among the three strain values. When the acceleration was between 20 g and

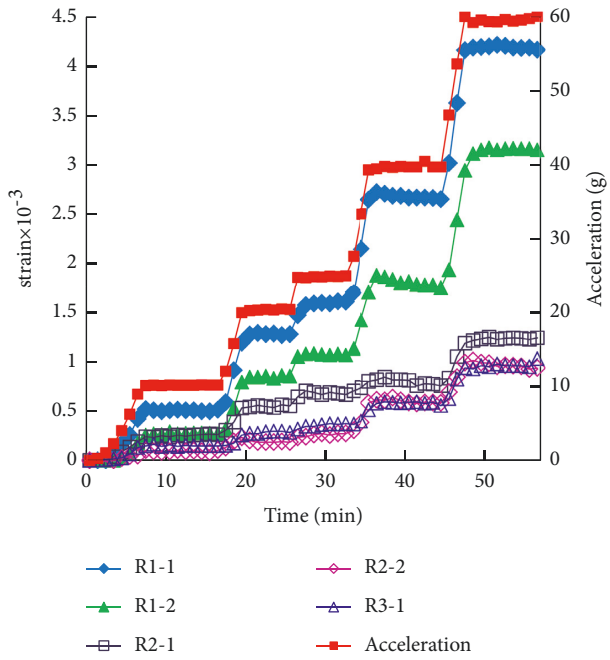

Figure 10: Geogrid strain in RS3 model.

50 g, the largest geogrid strain was found in the bottom section, followed by the middle section, and the smallest strain was found in the upper section. For accelerations above 50 g, the largest geogrid strain was still found in the bottom section, whereas the strain in the upper section was slightly larger than that in the middle section.

The spacing in the RS2 reinforced slope model was relatively small. The maximum strain in the geogrid in this model was smaller than those in the RS3 and RS4 models, both of which had relatively large reinforcement spacings. Thus, within a certain range, the greater was the number of reinforcement layers, the smaller was the force on the geogrid at the same position, and the more significant was the reinforcing effect on the soil. The geogrid stress in the lower section of the embankment was significantly larger than that in the upper section. Therefore, in the design stage, comparatively fewer reinforcements should be placed in the upper section than in the lower section. For equally spaced reinforcements, the geogrid should be strengthened in the middle and lower sections.

Phenomena, such as overall slope collapse and geogrid fracture, were not observed in any of the reinforced embankment centrifuge models. When the slope of a geogrid-gravelly-soil-reinforced steep slope embankment failed, the soil first reached the limit state, followed by relative sliding between the reinforcement and the soil, and the soil-reinforcement interface reached the limit state. During the entire test, the geogrid did not fracture or reach the limit state. The geogrid barred the formation of a continuous sliding surface in the soil. The main reason for embankment failure was the continuous relative displacement between the reinforcement and the soil. The resulting continuous increase in the displacement at the crest and the surface of the slope then led to progressive failure. The geogrid

(a) (b)

Figure 11: Photographs of RS4 embankment centrifuge model after test. (a) Side view. (b) Top view.

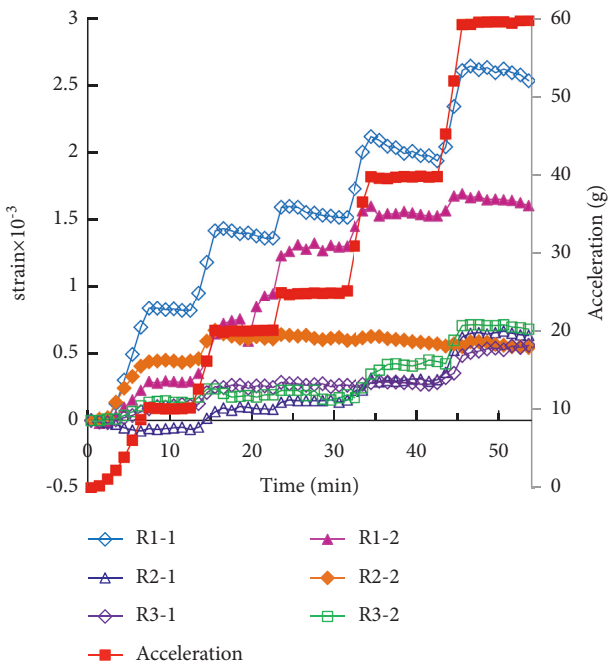

Figure 12: Geogrid strain in RS4 model.

reinforcement thus significantly changed the failure mode of the slope from that of the unreinforced slope. Considering the engineering economy and construction difficulty, it is better to choose the geogrid with relatively smaller spacing and lower strength than the geogrid with larger spacing and higher strength.

From the RS2 and RS4 tests, it can be seen that, compared with other parts of the slope, the soil between the two layers of grids was the weakest part of the entire reinforced structure. In the RS2 test, the reinforcement spacing was 5 cm, while that in the RS4 test was 10 cm, and the former was only 1/2 of the latter. In addition, the number of reinforcement layers in the RS2 test was also greater than that in the RS4 test. This finding shows that the arrangement of reinforcement, the number of layers, and the spacing of reinforcement layers in the grid-reinforced structure have a great influence on the reinforcement effect. A typical dense reinforcement state was achieved in the RS2 test, and the RS4 test was in a typical sparse reinforcement state. When the reinforced structure was subject to a sparse reinforcement, the soil between the two layers of reinforcement was analyzed. It was found that the reinforcement effect on the soil between the two layers of reinforcement was poor. There was an obvious weak layer between the two layers of the reinforcement. When the reinforced structure experienced a dense reinforcement, the soil between the two layers of grids was reinforced, and the strength of the reinforcement was improved as a whole. There was no weak part in the soil between the upper and lower layers of reinforcement. Even with the increase of gravity acceleration, the soil mass between the reinforcement bars was cracked, and a barrier of the reinforcement bar to the soil mass cracks can inhibit the continuous development or expansion of cracks.

The influence range of geogrid on soil was about 6-7 times of the average particle size of soil particles under different vertical loads. In the RS2 test, the spacing of the grid layers was smaller than the influence range of the geogrid on the soil. The interlayer spacing in the RS3 test was equivalent to the upper limit of the thickness of the influence zone, and the interlayer spacing in the RS4 test was greater than the thickness of the influence zone. Within the influence zone, the distributed force caused by the friction-like force between the geogrid and the soil had a reinforcing effect on the soil. Outside the influence zone, this distributed force gradually decayed to zero with increasing distance from the grid, and the soil remains in its original stress state. In the RS2 test, the distribution forces of the soil caused by the friction force on the two adjacent layers of geogrids overlapped and influenced each other and played a role in strengthening the soil in the entire reinforcement range of the slope. In the RS3 and RS4 tests, the distribution forces of the soil caused by the frictional force of the adjacent two geogrids failed to overlap each other. Especially in the RS4 test, there were some soil layers unaffected by the distribution force of the soil between the two layers of geogrids. These soil layers became the weak parts of the entire slope. With an increase in centrifugal acceleration, the soil in these layers first reached the plastic state and failed, resulting in a large lateral displacement. According to the current design

method, in the design of reinforced steep slopes, when geogrids with different tensile strengths were selected, the interlayer spacing of geogrids also differed.

According to the current design method, the layer spacing of geogrid differs when geogrids with different tensile strengths are selected in the design of a reinforced steep slope. Centrifugal model test results show that an excessive vertical spacing of geogrid in a reinforced steep slope may lead to an excessive deformation of the slope, and even lead to a global failure of the slope. For a reinforced embankment with a height less than 20 m, considering the engineering economy and construction difficulty, a geogrid with smaller spacing and lower strength is better than a geogrid with larger spacing and higher strength.

4. Conclusions

Two centrifuge model tests were conducted to simulate a steep slope embankment with and without a geogrid gravelly soil reinforcement. The failure mechanism of the slope was elucidated. The main conclusions of the study are given below.

(1) Centrifuge test is an effective model test method. Under a centrifugal force, the unreinforced gravelly soil steep slope embankment failed in sudden collapse and circular sliding. The reinforced embankment exhibited a local deformation on the slope surface and a continuous progressive deformation due to the failure of geogrid-soil interface.

(2) The centrifuge tests showed that the geogrid reinforcement had a reinforcing effect on the soil and enhanced the integrity of the embankment, thereby improving the slope stability and reducing the horizontal lateral displacement of the slope and the settlement of the slope crest. The geogrid arrangement, number of layers, and reinforcement layer spacing significantly influenced the reinforcement performance of a geogrid-reinforced structure.

(3) In the centrifugal model test of a geogrid-reinforced steep slope embankment, with an increase in centrifugal acceleration, the soil between the two layers of geogrids in the slope first reaches the plastic state and subsequently fails, resulting in a large lateral displacement. In the design of reinforced steep slopes, when geogrids with different tensile strengths are selected, the interlayer spacing of geogrids differs.

(4) The stress of a geogrid-reinforced steep embankment in the lower section of the embankment was significantly larger than that in the upper section. In the design of a geogrid, reinforcements should be sparsely arranged in the upper section and densely arranged in the lower section. For equally spaced reinforcements, the geogrid should be strengthened in the middle and lower sections.

Data Availability

The data used to support the findings of this study are included in the article.

Conflicts of Interest

The authors declare that there are no conflicts of interest in this study.

Authors' Contributions

Jie Liu and Yunlong Sun made the same contribution to this paper and are both first authors.

Acknowledgments

This paper was funded by the Anhui Natural Science Foundation (No. KJ2014A092) and the Transportation Science and Technology Project of Xinjiang Uygur Autonomous Region (No. KY2019020).

References

[1] M. S. S. Almeida, D. F. Fagundes, L. Thorel, and M. Blanc, "Geosynthetic-reinforced pile-embankments: numerical, analytical and centrifuge modelling," *Geosynthetics International*, vol. 27, no. 3, pp. 1–37, 2019.

[2] S. Balakrishnan and B. V. S. Viswanadham, "Performance evaluation of geogrid reinforced soil walls with marginal backfills through centrifuge model tests," *Geotextiles and Geomembranes*, vol. 44, no. 1, pp. 95–108, 2016.

[3] W. Cui and M. Xiao, "Centrifuge modeling of geogrid-reinforced and rammed soil-cement column-supported embankment on soft soil," *Journal of Testing and Evaluation*, vol. 48, no. 5, Article ID 20170603, 2020.

[4] S. Feng, R. Xu, K. Cheng, J. Yu, and Q. Jia, "Centrifuge model test on the performance of geogrid-reinforced and pile-supported embankment over soft soil," *Soil Mechanics and Foundation Engineering*, vol. 57, no. 3, pp. 244–251, 2020.

[5] A. Kyparissis and M. P. Lopes, "Bearing capacity of reinforced soil under a strip footing: centrifuge tests," in *Proceedings of the 11th International Conference on Geosynthetics*, Seoul, Korea, September 2018.

[6] J. Mamaghanian, B. Viswanadham, and H. R. Razeghi, "Centrifuge model studies on geocomposite reinforced soil walls subjected to seepage," *Geosynthetics International*, vol. 26, no. 4, pp. 371–387, 2019.

[7] H. Razeghi, B. Viswanadham, and J. Mamaghanian, "Centrifuge and numerical model studies on the behaviour of geogrid reinforced soil walls with marginal backfills with and without geocomposite layers," *Geotextiles and Geomembranes*, vol. 47, no. 5, pp. 671–684, 2019.

[8] P. Shen, C. Xu, and J. Han, "Centrifuge tests to investigate global performance of geosynthetic-reinforced pile-supported embankments with side slopes," *Geotextiles and Geomembranes*, vol. 48, no. 1, pp. 120–127, 2020.

[9] H.. , X. R. Xu, J. N. Chen, C. N. Liu, L. Xia, and Y. W. Liu, "Centrifuge model tests of geogrid-reinforced slope

supporting a high embankment," *Geosynthetics International*, vol. 26, no. 6, pp. 629–640, 2019.

[10] C. Xu, Y.-S. Luo, B. Jia, and H.-S. Chen, "Effects of connection forms on shored mechanically stabilized earth walls by centrifugal model tests," *Chinese Journal of Geotechnical Engineering*, vol. 38, pp. 180–186, 2016.

[11] W. Zhang, J. F. Chen, and Y. Yu, "Influence of toe restraint conditions on performance of geosynthetic- reinforced soil retaining walls using centrifuge model tests," *Geotextiles and Geomembranes*, vol. 47, no. 5, pp. 653–661, 2019.

[12] D. Bhattacherjee and B. Viswanadham, "Centrifuge model studies on performance of hybrid geosynthetic-reinforced slopes with poorly draining soil subjected to rainfall," *Journal of Geotechnical and Geoenvironmental Engineering*, vol. 145, no. 12, 2019.